

Slepton pair production with aNNLO+NNLL precision

Juri Fiaschi,^a Michael Klasen^a and Marthijn Sunder^a

^a*Institut für Theoretische Physik, Westfälische Wilhelms-Universität Münster, Wilhelm-Klemm-Straße 9, D-48149 Münster, Germany*

E-mail: fiaschi@uni-muenster.de, michael.klasen@uni-muenster.de,
mpasunder@uni-muenster.de

ABSTRACT: We present a calculation of slepton pair production at the LHC at next-to-next-to-leading logarithmic (NNLL) accuracy, matched to approximate next-to-next-to-leading order (aNNLO) QCD corrections. We collect the relevant analytical formulae, discuss the matching of logarithmically enhanced and fixed-order results and describe the transformation of parton densities and hadronic cross sections to and from Mellin space. Numerically, we find a moderate increase of invariant-mass distributions and total cross sections with respect to our previous results at next-to-leading logarithmic (NLL) accuracy matched to next-to-leading order (NLO), and more importantly a further significant reduction of the factorisation and renormalisation scale dependence that stabilises our predictions to the permil level. The dependence on other supersymmetric parameters like squark and gluino masses and sbottom mixing that enter only at NLO is found to be weak, i.e. less than two percent, as expected.

KEYWORDS: Perturbative QCD, resummation, supersymmetry, hadron colliders

Contents

1	Introduction	1
2	Analytical approach	2
2.1	Threshold resummation at NNLL accuracy	3
2.2	Hard matching coefficients up to NNLO	4
2.3	Fixed-order matching and inverse Mellin transform	5
3	Numerical results for slepton pair production	7
3.1	Input parameters	7
3.2	Invariant-mass distributions	8
3.3	Total cross sections	9
4	Conclusion	14

1 Introduction

The search for supersymmetric (SUSY) particles is an important current research topic at CERN’s Large Hadron Collider (LHC). The reason is that SUSY is a well-motivated extension of the Standard Model (SM) of particle physics that can solve a significant number of shortcomings of this model. Important examples of SUSY solutions to SM problems are the stabilisation of the Higgs boson mass and a possible candidate for dark matter, which typically is the lightest neutralino, a mixture of the fermionic partners of the neutral electroweak gauge and Higgs bosons [1, 2]. Sleptons, the scalar partners of the SM leptons, are usually also among the lightest SUSY particles [3]. While LHC searches already constrain squarks and gluinos, the SUSY partners of quarks and gluons, to the mass range above 1 or 2 TeV [4, 5], the limits on left-handed selectron and smuon masses are less stringent and lie at 550 and 560 GeV, respectively [6, 7]. Staus can even be as light as 390 GeV [8, 9].

Experimental SUSY searches at the LHC rely on precise theoretical predictions that go beyond leading order (LO) in perturbative QCD [10, 11] and include not only next-to-leading order (NLO) QCD [12] and SUSY-QCD corrections [13], but that also resum the contributions that are logarithmically enhanced. These enhancements can otherwise spoil the convergence of the perturbative series. They occur at small transverse momenta of the produced slepton pair [14], close to the production threshold [15, 16], or both [17]. Threshold resummation corrections not only increase the production cross section, thereby enhancing the discovery ranges or exclusion limits, but also reduce its dependence on the unphysical factorisation and renormalisation scales and thus render the theoretical predictions more accurate. Together with resummation-improved parton density functions

(PDFs) [18], also the PDF uncertainty can in principle be reduced [19, 20], even though in practice these PDFs must currently be fitted to smaller data sets than global NLO analyses and thus still have larger errors. Similar calculations have been performed for gaugino and higgsino pairs [21–26], gluinos and gauginos [27, 28], and additional gauge bosons [29–32], are available within the public code RESUMMINO [33] and are regularly employed in the experimental analyses by ATLAS [34] and CMS [35]. Predictions have also recently been made for the high-luminosity (HL) and high-energy (HE) phases of the LHC [36].

In this paper, we take our precision calculations for slepton pair production to the next level by resumming not only the leading and next-to-leading logarithms (NLL), but also the next-to-next-to-leading logarithms (NNLL) and matching them not only to the full NLO QCD and SUSY-QCD corrections, but also an approximate next-to-next-to-leading order (aNNLO) calculation in QCD. The corresponding analytical formulae are available in the literature [37–39] and are collected here to make the paper self-contained. Similar calculations, based on full NLO SUSY-QCD calculations [40, 41], have also been performed previously for squarks and gluinos [42] and stops [43] and are available through the public code NNLL-fast [44].

The paper is organised as follows: In Sec. 2, we describe our analytical approach and in particular how threshold logarithms can be resummed at NNLL accuracy, matched to a fixed-order calculation up to NNLO and how the PDFs and hadronic cross sections are transformed to and from Mellin space. Our numerical results are contained in Sec. 3. This section starts with a discussion of the QCD and SUSY input parameters, followed by a demonstration of how the NNLL and aNNLO contributions affect the differential cross section in particular at high invariant masses. We then show the effects of the new contributions on the total cross section, its dependence on the factorisation and renormalisation scales as well as on other SUSY parameters like the squark and gluino masses or the trilinear coupling governing squark mixing in the bottom sector. The ensuing conclusions are presented in Sec. 4.

2 Analytical approach

The hadronic invariant mass distribution for the production of slepton pairs,

$$M^2 \frac{d\sigma_{AB}}{dM^2}(\tau) = \sum_{a,b} \int_0^1 dx_a dx_b dz [x_a f_{a/A}(x_a, \mu_F^2)] [x_b f_{b/B}(x_b, \mu_F^2)] \times [z\sigma_{ab}(z, M^2, \mu_R^2, \mu_F^2)] \delta(\tau - x_a x_b z), \quad (2.1)$$

is obtained from a convolution of the parton density functions (PDFs) $f_{a,b/A,B}$, that depend on the longitudinal momentum fractions $x_{a,b}$ of the partons a, b in the external hadrons A, B and the factorisation scale μ_F , with the partonic cross section σ_{ab} , that depends on the squared invariant mass of the produced sleptons M^2 , its ratio $z = M^2/s$ (whereas $\tau = M^2/S$) to the partonic (hadronic) center-of-mass energy s (S), and the renormalisation and factorisation scales μ_R and μ_F , respectively.

While the leading order (LO) cross section [10, 11] and the virtual next-to-leading order (NLO) corrections are proportional to $\delta(1-z)$ [12, 13], the kinematic mismatch in

the cancellation of infrared divergences among the virtual and real corrections of order n introduces large logarithmic remainders proportional to

$$\alpha_s^n(\mu_R^2) \left[\frac{\ln^m(1-z)}{1-z} \right]_+, \text{ where } m \leq 2n-1, \quad (2.2)$$

which close to threshold ($z \rightarrow 1$) spoil the convergence of the perturbative series in α_s and therefore have to be resummed to all orders [45, 46]. After performing a Mellin transformation,

$$F(N) = \int_0^1 dy y^{N-1} F(y), \quad (2.3)$$

of the PDFs and partonic cross section in Eq. (2.1), the hadronic cross section σ_{AB} factorises, the singular terms in Eq. (2.2) turn into large logarithms of the Mellin variable N ,

$$\left[\frac{\ln^m(1-z)}{1-z} \right]_+ \rightarrow \ln^{m+1} N + \dots, \quad (2.4)$$

and the partonic cross section σ_{ab} can be written in the exponentiated form

$$\sigma_{ab}^{(\text{res.})}(N, M^2, \mu_R^2, \mu_F^2) = H_{ab}(M^2, \mu_R^2, \mu_F^2) \exp[G_{ab}(N, M^2, \mu_R^2, \mu_F^2)] + \mathcal{O}\left(\frac{1}{N}\right). \quad (2.5)$$

Here, the exponent G_{ab} is universal and contains all the logarithmically enhanced contributions in the Mellin variable N , while the hard function H_{ab} is independent of N , though process-dependent.

2.1 Threshold resummation at NNLL accuracy

Up to next-to-next-to-leading logarithmic (NNLL) accuracy, the exponent G_{ab} can be written as

$$G_{ab}(N, M^2, \mu_R^2, \mu_F^2) = LG_{ab}^{(1)}(\lambda) + G_{ab}^{(2)}(\lambda, M^2, \mu_R^2, \mu_F^2) + \alpha_s G_{ab}^{(3)}(\lambda, M^2, \mu_R^2, \mu_F^2), \quad (2.6)$$

where $\lambda = \alpha_s b_0 L$ and $L = \ln \bar{N} = \ln(Ne^{\gamma_E})$. The coefficients of the QCD β -function are denoted by $b_n = \beta_n/(2\pi)^{n+1}$, and the first three coefficients are given by [47, 48]

$$b_0 = \frac{1}{12\pi}(11C_A - 2n_f), \quad (2.7)$$

$$b_1 = \frac{1}{24\pi^2}(17C_A^2 - 5C_A n_f - 3C_F n_f), \quad (2.8)$$

$$b_2 = \frac{1}{64\pi^3} \left(\frac{2857}{54} C_A^3 - \frac{1415}{54} C_A^2 n_f - \frac{205}{18} C_A C_F n_f + C_F^2 n_f + \frac{79}{54} C_A n_f^2 + \frac{11}{9} C_F n_f^2 \right) \quad (2.9)$$

with $C_A = N_C = 3$, $C_F = (N^2 - 1)/(2N_C) = 4/3$ and the number of active quark flavours $n_f = 5$. For Drell-Yan-like processes such as slepton or gaugino pair production initiated by quarks and antiquarks only, the coefficients $G_{ab}^{(i)} = g_a^{(i)} + g_b^{(i)}$ with $a = b = q$ can, e.g., be

found up to next-to-leading logarithmic (NLL) accuracy in Refs. [15, 22]. At NNLL, one also needs [37]

$$\begin{aligned}
g_q^{(3)}(\lambda) &= \frac{A^{(1)}b_1^2}{2\pi b_0^4} \frac{1}{1-2\lambda} \left[2\lambda^2 + 2\lambda \ln(1-2\lambda) + \frac{1}{2} \ln^2(1-2\lambda) \right] \\
&+ \frac{A^{(1)}b_2}{2\pi b_0^3} \left[2\lambda + \ln(1-2\lambda) + \frac{2\lambda^2}{1-2\lambda} \right] + \frac{2A^{(1)}}{\pi} \zeta_2 \frac{\lambda}{1-2\lambda} \\
&- \frac{A^{(2)}b_1}{(2\pi)^2 b_0^3} \frac{1}{1-2\lambda} \left[2\lambda^2 + 2\lambda + \ln(1-2\lambda) \right] + \frac{A^{(3)}}{\pi^3 b_0^2} \frac{\lambda^2}{1-2\lambda} - \frac{D^{(2)}}{2\pi^2 b_0} \frac{\lambda}{1-2\lambda} \\
&+ \frac{A^{(1)}b_1}{2\pi b_0^2} \frac{1}{1-2\lambda} \left[2\lambda + \ln(1-2\lambda) \right] \ln \left(\frac{M^2}{\mu_R^2} \right) + \frac{A^{(1)}}{2\pi} \left[\frac{\lambda}{1-2\lambda} \ln^2 \left(\frac{M^2}{\mu_R^2} \right) - \lambda \ln^2 \left(\frac{\mu_F^2}{\mu_R^2} \right) \right] \\
&- \frac{A^{(2)}}{2\pi^2 b_0} \left[\frac{\lambda}{1-2\lambda} \ln \left(\frac{M^2}{\mu_R^2} \right) - \lambda \ln \left(\frac{\mu_F^2}{\mu_R^2} \right) \right]. \tag{2.10}
\end{aligned}$$

Here, the universal process-independent coefficients are given by [49]

$$A^{(1)} = 2C_F, \tag{2.11}$$

$$A^{(2)} = 2C_F \left[C_A \left(\frac{67}{18} - \zeta_2 \right) - \frac{5}{9} n_f \right], \tag{2.12}$$

$$\begin{aligned}
A^{(3)} &= \frac{1}{2} C_F \left[C_A^2 \left(\frac{245}{24} - \frac{67}{9} \zeta_2 + \frac{11}{6} \zeta_3 + \frac{11}{5} \zeta_2^2 \right) + C_F n_f \left(2\zeta_3 - \frac{55}{24} \right) \right. \\
&\quad \left. + C_A n_f \left(\frac{10}{9} \zeta_2 - \frac{7}{3} \zeta_3 - \frac{209}{108} \right) - \frac{n_f^2}{27} \right] \tag{2.13}
\end{aligned}$$

and [37]

$$D^{(2)} = 2C_F \left[C_A \left(-\frac{101}{27} + \frac{11}{3} \zeta_2 + \frac{7}{2} \zeta_3 \right) + n_f \left(\frac{14}{27} - \frac{2}{3} \zeta_2 \right) \right]. \tag{2.14}$$

2.2 Hard matching coefficients up to NNLO

The hard N -independent part of the Mellin-transformed partonic cross section in Eq. (2.5),

$$H_{ab}(M^2, \mu_R^2, \mu_F^2) = \sigma_{ab}^{(0)} \mathcal{C}_{ab}(M^2, \mu_R^2, \mu_F^2), \tag{2.15}$$

can be perturbatively expanded in terms of the Mellin-transformed LO cross section $\sigma_{ab}^{(0)}$ and

$$\mathcal{C}_{ab}(M^2, \mu_R^2, \mu_F^2) = \sum_{n=0} \left(\frac{\alpha_s}{2\pi} \right)^n \mathcal{C}_{ab}^{(n)}(M^2, \mu_R^2, \mu_F^2), \tag{2.16}$$

where the hard matching coefficients

$$\mathcal{C}_{ab}^{(n)}(M^2, \mu_R^2, \mu_F^2) = \left(\frac{2\pi}{\alpha_s} \right)^n \left[\frac{\sigma_{ab}^{(n)}}{\sigma_{ab}^{(0)}} \right]_{\text{N-ind.}} \tag{2.17}$$

are obtained from the finite (N -independent) terms in the ratio of the n -th order cross section over the LO one. The coefficients up to next-to-next-to-leading order (NNLO) can

be obtained from Refs. [38, 39] and are given by

$$\mathcal{C}_{ab}^{(0)} = 1, \quad (2.18)$$

$$\mathcal{C}_{ab}^{(1)} = C_F \left[\frac{4}{3}(\pi^2 - 6) - 3 \log \left(\frac{\mu_F^2}{M^2} \right) \right], \quad (2.19)$$

$$\begin{aligned} \mathcal{C}_{ab}^{(2)} = & \frac{C_F}{720} \left\{ 5(-4605C_A + 4599C_F + 762n_f) + 20\pi^2(188C_A - 297C_F - 32n_f) \right. \\ & - 92\pi^4(C_A - 6C_F) + 180(11C_A + 18C_F - 2n_f) \log^2 \left(\frac{\mu_F^2}{M^2} \right) \\ & - 160(11C_A - 2n_f)(6 - \pi^2) \log \left(\frac{\mu_R^2}{M^2} \right) + 80(151C_A - 135C_F + 2n_f)\zeta_3 \\ & + 20 \log \left(\frac{\mu_F^2}{M^2} \right) \left[-51C_A + 837C_F + 6n_f - 4\pi^2(11C_A + 27C_F - 2n_f) \right. \\ & \left. \left. + (-198C_A + 36n_f) \log \left(\frac{\mu_R^2}{M^2} \right) + 216(C_A - 2C_F)\zeta_3 \right] \right\}. \end{aligned} \quad (2.20)$$

By including the coefficients up to NNLO, the resummation of logarithmically enhanced contributions is improved, since also beyond NNLO in α_s the finite terms are multiplied by threshold logarithms.

2.3 Fixed-order matching and inverse Mellin transform

Although near to threshold the resummed cross section is a valid approximation, outside this region the normal perturbative calculation should be used. A reliable prediction in all kinematic regions is then obtained through a consistent matching of the two results with

$$\sigma_{ab} = \sigma_{ab}^{(\text{res.})} + \sigma_{ab}^{(\text{f.o.})} - \sigma_{ab}^{(\text{exp.})}. \quad (2.21)$$

Here, the resummed cross section $\sigma_{ab}^{(\text{res.})}$ in Eq. (2.5) has been re-expanded to NNLO, yielding $\sigma_{ab}^{(\text{exp.})}$, and subtracted from the fixed-order calculation $\sigma_{ab}^{(\text{f.o.})}$ in order to avoid the double counting of the logarithmically enhanced contributions. At $\mathcal{O}(\alpha_s^2)$ we then obtain

$$\begin{aligned} \sigma_{ab}^{(\text{exp.})}(N, M^2, \mu_R^2, \mu_F^2) &= \sigma_{ab}^{(0)} \mathcal{C}_{ab}(M^2, \mu_R^2, \mu_F^2) \exp[G_{ab}(N, M^2, \mu_R^2, \mu_F^2)] \\ &= \sigma_{ab}^{(0)} \left[1 + \left(\frac{\alpha_s}{2\pi} \right) \mathcal{C}_{ab}^{(1)} + \left(\frac{\alpha_s}{2\pi} \right)^2 \mathcal{C}_{ab}^{(2)} + \dots \right] \left[1 + \left(\frac{\alpha_s}{2\pi} \right) \mathcal{K}^{(1)} + \left(\frac{\alpha_s}{2\pi} \right)^2 \mathcal{K}^{(2)} + \dots \right] \\ &= \sigma_{ab}^{(0)} \left[1 + \left(\frac{\alpha_s}{2\pi} \right) (\mathcal{C}_{ab}^{(1)} + \mathcal{K}^{(1)}) + \left(\frac{\alpha_s}{2\pi} \right)^2 (\mathcal{C}_{ab}^{(2)} + \mathcal{K}^{(2)} + \mathcal{C}_{ab}^{(1)} \mathcal{K}^{(1)}) + \dots \right]. \end{aligned} \quad (2.22)$$

The coefficients of the expanded exponential term can be organised in powers of L as

$$\mathcal{K}^{(1)} = \mathcal{K}^{(1,1)} L + \mathcal{K}^{(1,2)} L^2, \quad (2.23)$$

$$\mathcal{K}^{(2)} = \mathcal{K}^{(2,1)} L + \mathcal{K}^{(2,2)} L^2 + \mathcal{K}^{(2,3)} L^3 + \mathcal{K}^{(2,4)} L^4. \quad (2.24)$$

Explicitly, they are given by [38, 39]

$$\mathcal{K}^{(1,1)} = 4C_F \log\left(\frac{\mu_F^2}{s}\right), \quad (2.25)$$

$$\mathcal{K}^{(1,2)} = 4C_F, \quad (2.26)$$

$$\begin{aligned} \mathcal{K}^{(2,1)} = & -\frac{C_F}{27} \left\{ 56n_f - 404C_A + 3 \log\left(\frac{\mu_F^2}{s}\right) \left[20n_f + 2C_A(-67 + 3\pi^2) \right. \right. \\ & \left. \left. + 3(11C_A - 2n_f) \left(\log\left(\frac{\mu_F^2}{\mu_R^2}\right) - \log\left(\frac{\mu_R^2}{s}\right) \right) \right] + 378C_A\zeta_3 \right\}, \end{aligned} \quad (2.27)$$

$$\begin{aligned} \mathcal{K}^{(2,2)} = & \frac{2}{9}C_F \left[-10n_f + 67C_A - 3C_A\pi^2 + 36C_F \log^2\left(\frac{\mu_F^2}{s}\right) \right. \\ & \left. + (33C_A - 6n_f) \log\left(\frac{\mu_R^2}{s}\right) \right], \end{aligned} \quad (2.28)$$

$$\mathcal{K}^{(2,3)} = \frac{4}{9}C_F \left[11C_A - 2n_f + 36C_F \log\left(\frac{\mu_F^2}{s}\right) \right], \quad (2.29)$$

$$\mathcal{K}^{(2,4)} = 8C_F^2. \quad (2.30)$$

The SUSY-QCD (squark-gluino loop) corrections are only matched at NLO, since they are not known beyond this order [13]. In this sense, our results are accurate to approximate NNLO (aNNLO) plus NNLL precision. This approximation is justified by the fact that the SUSY-QCD corrections are subdominant due to the large squark and gluino masses.

Having computed the resummed and the perturbatively expanded results in Mellin space, we must multiply them with the N -moments of the PDFs and perform an inverse Mellin transform,

$$M^2 \frac{d\sigma_{AB}}{dM^2}(\tau) = \frac{1}{2\pi i} \int_{\mathcal{C}_N} dN \tau^{-N} M^2 \frac{d\sigma_{AB}(N)}{dM^2}, \quad (2.31)$$

in order to obtain the hadronic cross section as a function of $\tau = M^2/S$. Special attention must be paid to the singularities in the resummed exponents $G_{ab}^{(1,2,3)}$, which are situated at $\lambda = 1/2$ and are related to the Landau pole of the perturbative coupling α_s . In order to avoid this pole as well as those in the Mellin moments of the PDFs related to the small- x (Regge) singularity $f_{a/A}(x, \mu_0^2) \propto x^\alpha (1-x)^\beta$ with $\alpha < 0$, we choose an integration contour \mathcal{C}_N according to the *principal value* procedure proposed in Ref. [50] and the *minimal prescription* proposed in Ref. [51]. We define two branches,

$$\mathcal{C}_N : N = C + ze^{\pm i\phi} \quad \text{with } z \in [0, \infty[, \quad (2.32)$$

where the constant C is chosen such that the singularities of the N -moments of the PDFs lie to the left and the Landau pole to the right of the integration contour. Formally, the angle ϕ can be chosen in the range $[\pi/2, \pi[$, but the integral converges faster if $\phi > \pi/2$. The Mellin moments of the PDFs are obtained by fitting to the parameterisations tabulated in x -space the functional form used by the MSTW collaboration [52]

$$f(x) = A_0 x^{A_1} (1-x)^{A_2} \left(1 + A_3 \sqrt{x} + A_4 x + A_5 x^{\frac{3}{2}} \right) + A_6 x^2 + A_7 x^{\frac{5}{2}}, \quad (2.33)$$

which has the advantage that it can be transformed analytically with the result

$$\begin{aligned}
F(x) = & A_0 \Gamma(y) B'(A_1 + N, y) + A_3 B'\left(A_1 + N + \frac{1}{2}, y\right) + A_4 B'(A_1 + N + 1, y) \\
& + A_5 B'\left(A_1 + N + \frac{3}{2}, y\right) + A_6 B'(A_1 + N + 2, y) + A_7 B'\left(A_1 + N + \frac{5}{2}, y\right). \quad (2.34)
\end{aligned}$$

Here, $y = A_2 + 1$ and $B'(x, y) = B(x, y)/\Gamma(y) = \Gamma(x)/\Gamma(x + y)$. We verified that we obtain good fits not only for the MMHT2014NLO118 [52], but also for the CT14NLO fits [53] up to large values of x and for all typical factorisation scales, even though the latter are obtained with an ansatz that includes an exponential function.

3 Numerical results for slepton pair production

In this section, we present numerical results for slepton pair production at the LHC with aNNLO+NNLL precision. We first discuss our choice of input parameters and demonstrate the impact of threshold resummation on the invariant-mass distributions, after which we show and discuss our experimentally more relevant predictions for the total cross sections as a function of the slepton mass and other, subdominant SUSY parameters.

3.1 Input parameters

Our numerical results for proton-proton collisions at LHC Run 2 with a center-of-mass energy \sqrt{S} of 13 TeV have been obtained with CT14 PDFs [53], which we employ consistently at LO and NLO with the corresponding partonic cross sections. While the PDF uncertainty in resummation calculations can in principle be reduced by using also resummation-improved PDFs [19, 20], the latter are fitted to a substantially smaller data set than those at NLO, which unfortunately currently still results in a larger PDF uncertainty [18]. We therefore use here NLO PDFs with NLL and NNLL partonic cross sections and refer to Refs. [19, 20] for a detailed discussion of PDF uncertainties. Since top (s)quarks do not enter our calculations, all other five quark flavours are treated as massless, and the QCD scale parameter Λ is fixed accordingly to its CT14 values. For our central predictions, the renormalisation and factorisation scales are identified with the slepton mass. For scale uncertainty estimates, we employ the seven-point method, i.e. the scales are varied individually by relative factors of two, but not four.

Based on an integrated LHC luminosity of 139 (35.9) fb^{-1} and for sufficiently large mass differences with the lightest neutralino, the ATLAS (CMS) collaboration has recently excluded left-handed selectrons below 550 (400) GeV. For two (not three, as stated in the ATLAS abstract and conclusion) generations of mass-degenerate sleptons, the limit increases to 700 (450) GeV [6, 7]. We therefore adopt for the invariant-mass distributions a default slepton mass of 1 TeV and use 700 GeV as the lower mass limit for the total cross sections. Squarks and gluinos enter only at NLO in virtual loop diagrams, and therefore their masses play only a subdominant role. We adopt a squark and gluino mass of 1.3 TeV as our default value, which is still allowed for not too large mass differences with the lightest neutralino, even though the most stringent ATLAS (CMS) mass limits already

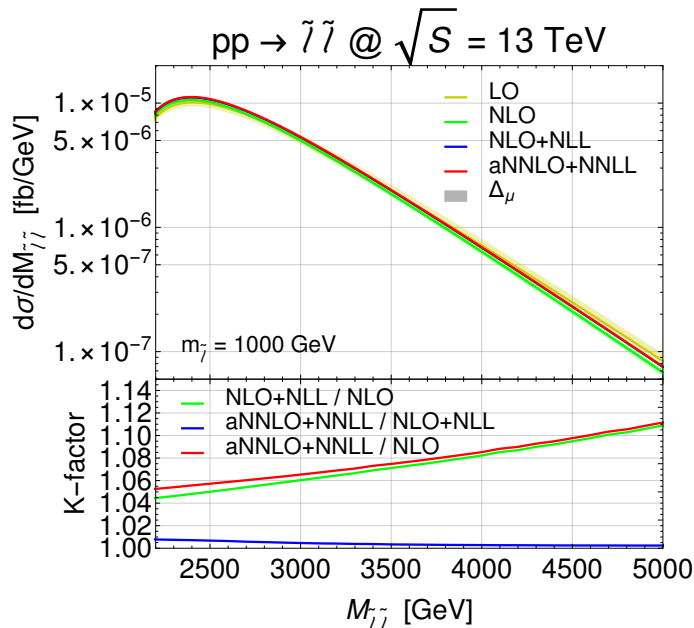


Figure 1. Top: Invariant-mass distribution for left-handed selectron (or smuon) pair production at the LHC with a center-of-mass energy of $\sqrt{S} = 13$ TeV for a fixed slepton mass of 1 TeV. Shown are results at LO (yellow), NLO (green), NLO+NLL (blue) and aNNLO+NNLL (red) together with the corresponding scale uncertainties (shaded bands). Bottom: Ratios (K factors) of NLO+NLL over NLO (green), aNNLO+NNLL over NLO+NLL (blue) and aNNLO+NNLL over NLO (red) differential cross sections as a function of the invariant mass of the slepton pair.

reach 1.94 (1.63) and 2.35 (2.31) TeV, respectively [4, 5]. We will study the dependence on these parameters up to 2.5 TeV and see that the dependence is indeed weak, as is the dependence on the mixing angle in the case of bottom squarks.

3.2 Invariant-mass distributions

In Fig. 1 (top) we plot the invariant-mass distributions for slepton pair production at the LHC with a center-of-mass energy of $\sqrt{S} = 13$ TeV and with LO (yellow), NLO (green), NLO+NLL (blue) and aNNLO+NNLL (red) precision together with the corresponding scale uncertainties (shaded bands). Since we do not take into account decays or detector acceptances, these results are valid for both left-handed selectrons and smuons of 1 TeV mass, while the cross sections for maximally mixed staus or right-handed selectrons and smuons are typically smaller by about a factor of 2 to 2.5 [19]. The cross section rises with the third power of the slepton velocity and peaks at an invariant mass that is considerably above the minimal value $2m_{\tilde{\ell}}$ before falling steeply off due to the s -channel propagator and the parton luminosity [15].

The effect of the higher-order corrections is best seen in Fig. 1 (bottom) as ratios (K factors) of NLO+NLL over NLO (green), aNNLO+NNLL over NLO+NLL (blue) and

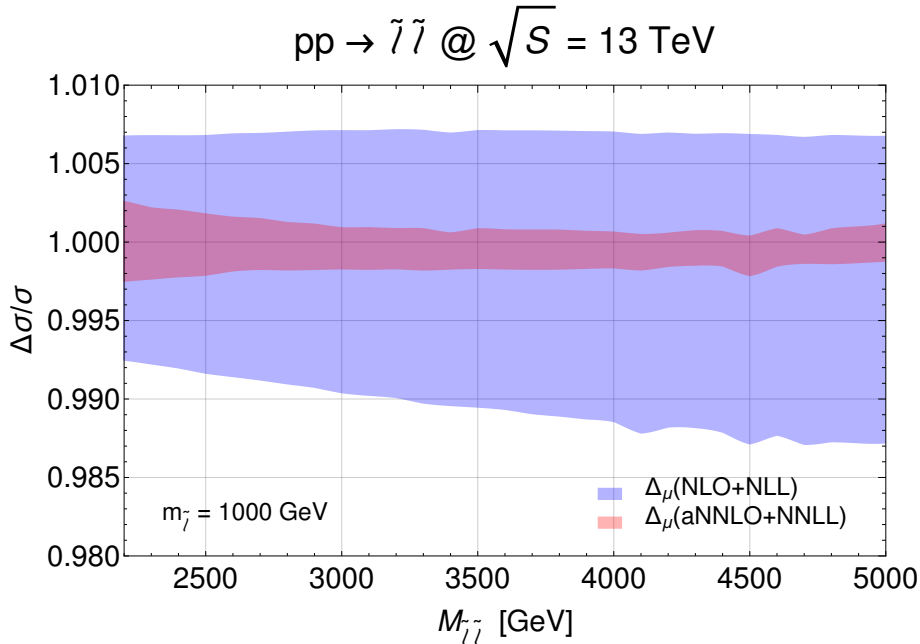


Figure 2. Scale uncertainty of the invariant-mass distribution for left-handed selectron (or smuon) pair production at the LHC with a center-of-mass energy of $\sqrt{S} = 13 \text{ TeV}$ for a fixed slepton mass of 1 TeV. Shown are the results at NLO+NLL (blue) and aNNLO+NNLL (red shaded band).

aNNLO+NNLL over NLO (red) differential cross sections. Resummation effects at NLL (green) accuracy become more important with respect to the fixed (NLO) order as the invariant mass of the slepton pair approaches the production threshold. The corresponding K factor increases in the invariant mass range of 2.2 to 5 TeV from 4.5% to 11%. The increase from NLO+NLL to aNNLO+NNLL is much smaller as expected for a converging expansion, and most visible at low invariant masses, where the constant terms at aNNLO induce an increase by about 1%.

Apart from the increase in cross section, which enhances the discovery range for new particles at the LHC, a second important effect of resummation calculations is the reduction in the theoretical uncertainty. It is estimated by varying the renormalisation and factorisation scales following the seven-point method. The result for the invariant mass distribution is shown in Fig. 2. While the uncertainty remained already mostly below one percent and exceeded this value very close to threshold at NLO+NLL (blue), the new contributions at aNNLO+NNLL (red shaded band) reduce the uncertainty considerably further to about one permil. Only at low invariant mass, i.e. far from threshold, the uncertainty rises to about two permil. This demonstrates the excellent stability of the expansion.

3.3 Total cross sections

We now turn to our predictions for total cross sections for slepton pair production at the LHC, which are directly applicable to determine experimental discovery ranges or exclusion limits. To this end, we plot in Fig. 3 (top) the total production cross section for left-handed

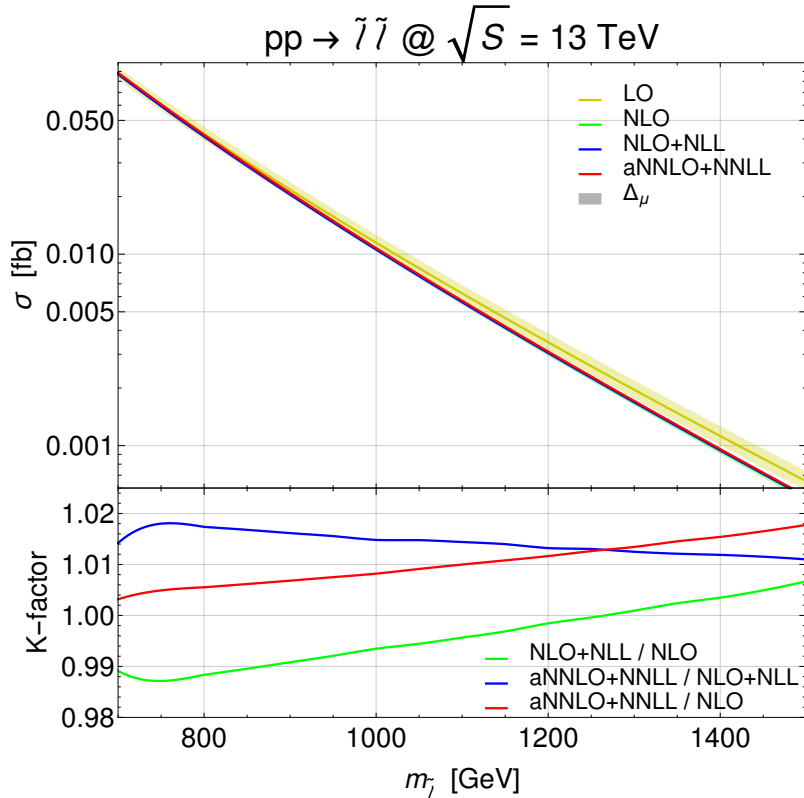


Figure 3. Top: Total cross section for left-handed selectron (or smuon) pair production at the LHC with a center-of-mass energy of $\sqrt{S} = 13$ TeV as a function of the slepton mass. Shown are results at LO (yellow), NLO (green), NLO+NLL (blue) and aNNLO+NNLL (red) together with the corresponding scale uncertainties (shaded bands). Bottom: Ratios (K factors) of NLO+NLL over NLO (green), aNNLO+NNLL over NLO+NLL (blue) and aNNLO+NNLL over NLO (red) total cross sections as a function of the slepton mass.

selectron (or smuon) pairs at the LHC with a center-of-mass energy of $\sqrt{S} = 13$ TeV as a function of the slepton mass in the range 700 GeV to 1500 GeV. In this range, the cross section falls from almost 0.1 fb to below 1 ab, corresponding to more than 10 events at 700 GeV with the currently analysed integrated luminosity of 139 fb^{-1} to 3 events at 1 TeV with the LHC Run 3 goal of 300 fb^{-1} and a few events at 1.5 TeV with the high-luminosity (HL) LHC goal of 3 ab^{-1} . The reduction of the scale uncertainty is visible as a decrease in width of the predictions from LO (yellow shaded band) to the higher orders (other colours).

The K factors in Fig. 3 (bottom) show that the logarithmic terms at NLL (green) and NNLL (red) first reduce, then enhance the cross section by a few percent with respect to the NLO prediction as the slepton mass increases. The aNNLO(+NNLL) terms lead in addition to an almost constant increase over the NLO(+NLL) prediction of about one percent (blue).

As for the invariant mass distribution, it is important to study the scale dependence

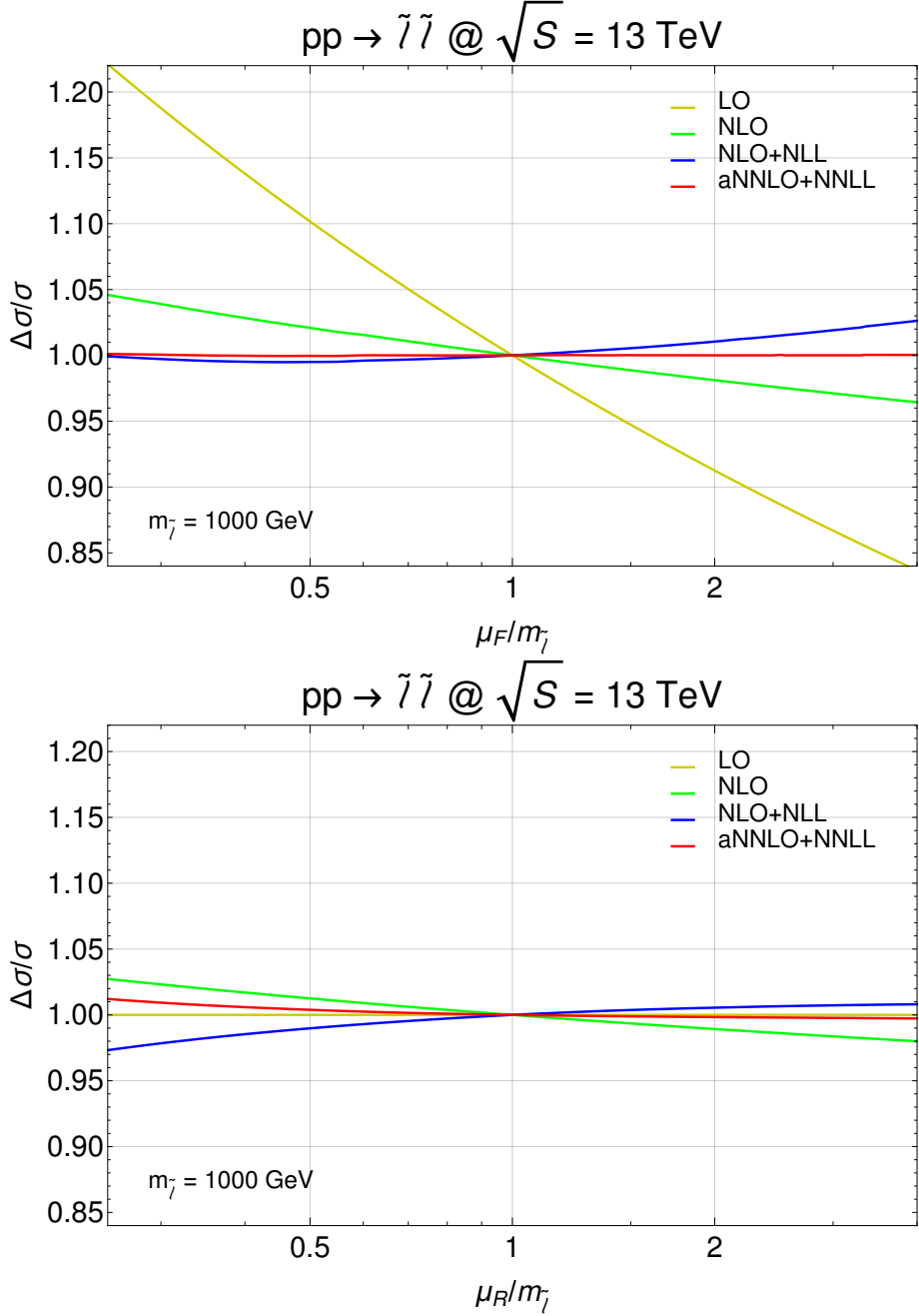


Figure 4. Relative variation of the total cross section for slepton pair production as function of the factorisation (top) and renormalisation scale (bottom). Shown are results at LO (yellow), NLO (green), NLO+NLL (blue) and aNNLO+NNLL (red).

at different levels of precision also for the total cross section. The variation of the total slepton pair production cross section at the LHC with 13 TeV center-of-mass energy with the factorisation scale is shown in Fig. 4 (top), normalised to the cross section at the central scale (the slepton mass of 1 TeV). The renormalisation scale is here fixed to this value.

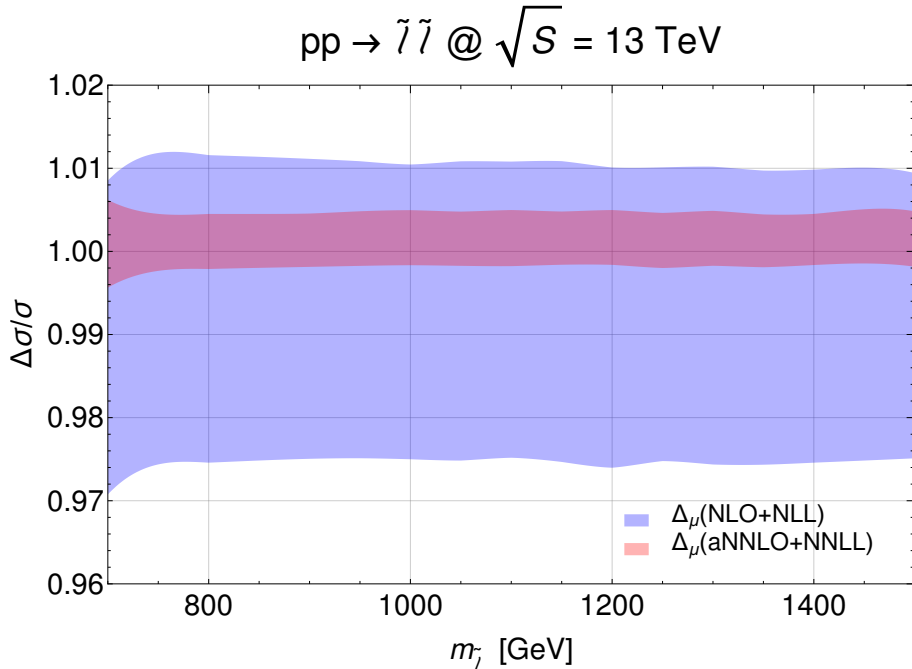


Figure 5. Scale uncertainty of the total cross section for left-handed selectron (or smuon) pair production at the LHC with a center-of-mass energy of $\sqrt{S} = 13 \text{ TeV}$ as a function of the slepton mass. Shown are the results at NLO+NLL (blue) and aNNLO+NNLL (red shaded band).

While we observe a steeply falling dependence from the PDFs at LO (yellow), it is already partially compensated at NLO through the factorisation of collinear divergences (green), further reduced and somewhat overcompensated at NLO+NLL (blue) and completely flat at aNNLO+NNLL (red).

Fig. 4 (bottom) shows the corresponding renormalisation scale dependence, where now the factorisation scale remains fixed. The dependence is only introduced at NLO, where $\alpha_s(\mu_R)$ falls with increasing scale (green), since the LO cross section is of electroweak origin (yellow). One then observes an oscillating behavior at NLO+NLL (blue) and aNNLO+NNLL (red) with a variation that is reduced from 5% at NLO to 1% at aNNLO+NNLL. This demonstrates again the excellent stability of the calculation.

The combined effect of varying the factorisation and renormalisation scales with the seven-point method is shown in Fig. 5 as a function of the slepton mass in the same range of 700 GeV to 1.5 TeV as considered above. We observe an almost constant theoretical uncertainty of -3% to $+1\%$ at NLO+NLL (blue), which is reduced to about -0.2% to $+0.4\%$ at aNNLO+NNLL (red shaded band) and which is only slightly larger for small slepton masses.

The virtual corrections at NLO do not only introduce a dependence on the renormalisation scale, but – through the squarks and gluinos appearing in the loops – also a weak dependence on other SUSY masses. Resumming logarithmically enhanced or adding approximate NNLO QCD, but not NNLO SUSY-QCD contributions does not alter this

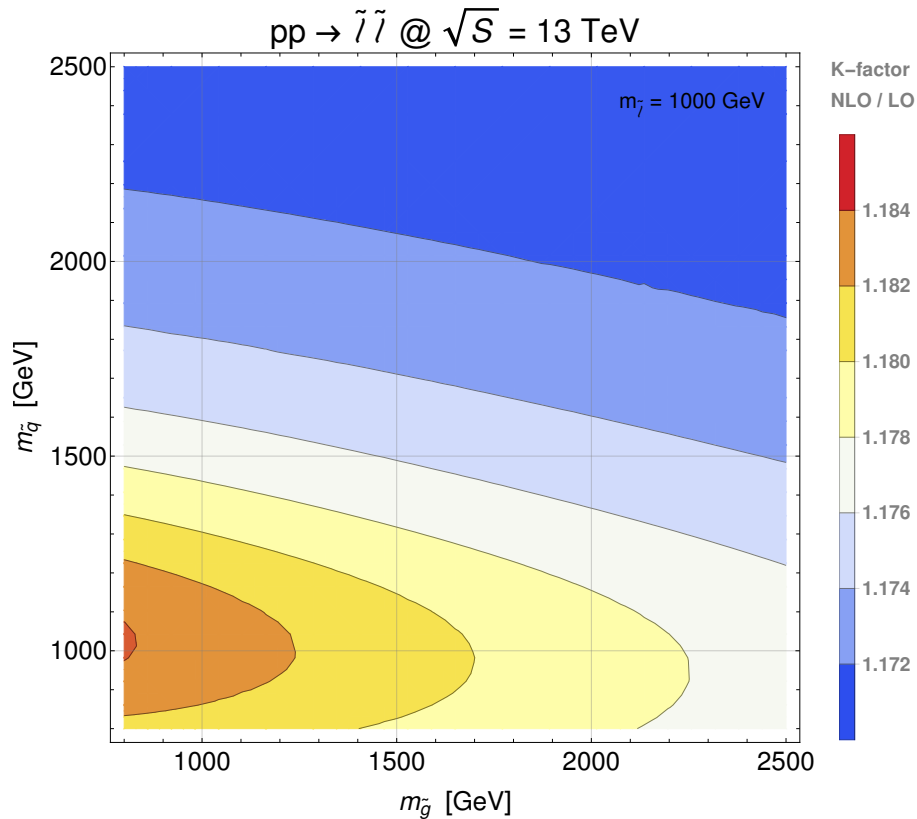


Figure 6. Ratio (K factor) of NLO over LO total cross sections (both with NLO PDFs) for left-handed selectron (or smuon) pair production at the LHC with a center-of-mass energy of $\sqrt{S} = 13$ TeV as a function of the squark and gluino masses.

dependence significantly. In Fig. 6 we show the impact of other SUSY masses on the slepton pair production cross section at the LHC as a colour-coded ratio of NLO over LO cross sections in the squark-gluino mass plane. Overall, the dependence is weak, as the K factor varies only from 1.170 to 1.186, i.e. by less than two percent. When the squark mass crosses the slepton mass at 1 TeV, the threshold behaviour in the triangle loop is clearly visible and represents the dominant dependence. The gluino mass appears only in the t -channel and is clearly less important. The squarks and gluinos decouple and no longer influence the cross section, when their masses reach the multi-TeV scale.

In simplified scenarios such as the phenomenological Minimal Supersymmetric Standard Model (pMSSM) [54, 55], it is common to assume a degeneracy of sfermion masses. For the first two generations, it is then a good approximation to do so also for the superpartners of the left- and right-handed fermions, since the off-diagonal terms in the sfermion mass matrix are proportional to the corresponding fermion mass. This is different for the third generation, where in the off-diagonal entries of the squark mass matrix the heavy-

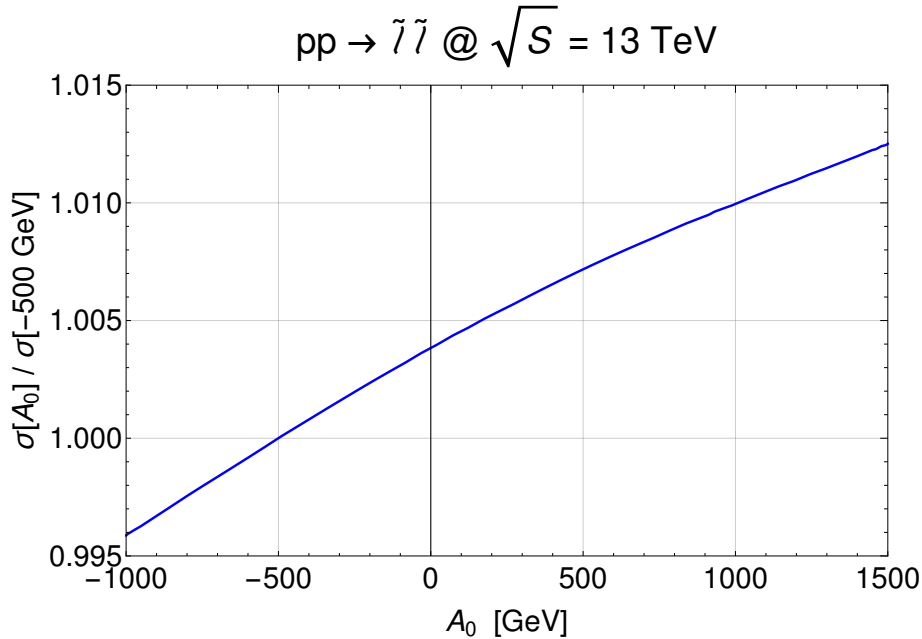


Figure 7. Dependence of the NLO (or NLO+NLL or aNNLO+NNLL) total cross section on the common trilinear coupling A_0 that governs squark mixing in the sbottom sector. Shown is the ratio over the default scenario with $A_0 = -500$ GeV.

quark masses m_t or m_b multiply the combinations

$$m_{LR} = A_0 - \mu^* \begin{cases} \cot \beta & \text{for up - type sfermions} \\ \tan \beta & \text{for down - type sfermions} \end{cases} \quad (3.1)$$

of the trilinear coupling A_0 , the higgsino mass parameter μ and the ratio of Higgs vacuum expectation values $\tan \beta = v_u/v_d$ for stops and sbottoms, respectively. While stops do not enter our calculations due to a negligible top quark PDF, sbottom mixing can influence slepton pair production at NLO. This is demonstrated in Fig. 7, where we show the dependence of the total slepton production cross section on the trilinear coupling A_0 normalised to the cross section at the default value of -500 GeV. The other relevant SUSY parameters have been set to $m_{LL} \simeq m_{RR} \simeq 1.1$ TeV, $\mu \simeq 0.8$ TeV and $\tan \beta = 40$. As expected, one observes an even weaker dependence of the NLO cross section on the sbottom mixing than on the squark and gluino masses, as it varies only from -0.4 to $+1.2$ percent.

4 Conclusion

In conclusion, we have presented in this paper a calculation of threshold resummation effects on slepton pair production at the LHC with NNLL accuracy matched to approximate NNLO QCD corrections. We collected the relevant analytical results from the literature and described the procedures, with which we matched resummation and fixed-order results and performed the transformation of PDFs and hadronic cross sections to and from Mellin

space. Numerically, we found only very moderate increases of invariant-mass distributions and total cross sections with respect to our previous calculations with NLO+NLL precision. More importantly, we observed very significant reductions on the renormalisation and factorisation scale dependences, that now stabilise our predictions to the permil level. We also discussed briefly the dependence of the cross section on squark and gluino masses that enter through virtual loop diagrams at NLO and demonstrated that our calculations are also applicable to mixing squarks, in particular of the third generation. Our results have been implemented in the code RESUMMINO and will soon become available with the next public release.

Acknowledgements

We thank B. Fuks for his collaboration on the off-diagonal squark loop contributions and N. Kidonakis for useful discussions. This work has been supported by the BMBF under contract 05H18PMCC1 and the DFG through the Research Training Network 2149 “Strong and weak interactions - from hadrons to dark matter”.

References

- [1] H. P. Nilles, *Phys. Rept.* **110**, 1 (1984).
- [2] H. E. Haber and G. L. Kane, *Phys. Rept.* **117**, 75 (1985).
- [3] J. A. Aguilar-Saavedra *et al.*, *Eur. Phys. J.* **C46**, 43 (2006), [arXiv:hep-ph/0511344 \[hep-ph\]](#) .
- [4] G. Aad *et al.* (ATLAS), (), [ATLAS-CONF-2019-040](#) .
- [5] A. M. Sirunyan *et al.* (CMS), [arXiv:1908.04722 \[hep-ex\]](#) .
- [6] G. Aad *et al.* (ATLAS), (), [arXiv:1908.08215 \[hep-ex\]](#) .
- [7] A. M. Sirunyan *et al.* (CMS), *Phys. Lett.* **B790**, 140 (2019), [arXiv:1806.05264 \[hep-ex\]](#) .
- [8] G. Aad *et al.* (ATLAS), (2019), [ATLAS-CONF-2019-018](#) .
- [9] A. M. Sirunyan *et al.* (CMS), (2019), [arXiv:1910.01185 \[hep-ex\]](#) .
- [10] S. Dawson, E. Eichten, and C. Quigg, *Phys. Rev.* **D31**, 1581 (1985).
- [11] G. Bozzi, B. Fuks, and M. Klasen, *Phys. Lett.* **B609**, 339 (2005), [arXiv:hep-ph/0411318 \[hep-ph\]](#) .
- [12] H. Baer, B. W. Harris, and M. H. Reno, *Phys. Rev.* **D57**, 5871 (1998), [arXiv:hep-ph/9712315 \[hep-ph\]](#) .
- [13] W. Beenakker, M. Klasen, M. Kramer, T. Plehn, M. Spira, and P. M. Zerwas, *Phys. Rev. Lett.* **83**, 3780 (1999), [Erratum: *Phys. Rev. Lett.*100,029901(2008)], [arXiv:hep-ph/9906298 \[hep-ph\]](#) .
- [14] G. Bozzi, B. Fuks, and M. Klasen, *Phys. Rev.* **D74**, 015001 (2006), [arXiv:hep-ph/0603074 \[hep-ph\]](#) .
- [15] G. Bozzi, B. Fuks, and M. Klasen, *Nucl. Phys.* **B777**, 157 (2007), [arXiv:hep-ph/0701202 \[hep-ph\]](#) .

- [16] B. Fuks, M. Klasen, D. R. Lamprea, and M. Rothering, *JHEP* **01**, 168 (2014), [arXiv:1310.2621](#) .
- [17] G. Bozzi, B. Fuks, and M. Klasen, *Nucl. Phys.* **B794**, 46 (2008), [arXiv:0709.3057 \[hep-ph\]](#) .
- [18] M. Bonvini, S. Marzani, J. Rojo, L. Rottoli, M. Ubiali, R. D. Ball, V. Bertone, S. Carrazza, and N. P. Hartland, *JHEP* **09**, 191 (2015), [arXiv:1507.01006 \[hep-ph\]](#) .
- [19] J. Fiaschi and M. Klasen, *JHEP* **03**, 094 (2018), [arXiv:1801.10357 \[hep-ph\]](#) .
- [20] J. Fiaschi and M. Klasen, in *2019 European Physical Society Conference on High Energy Physics (EPS-HEP2019) Ghent, Belgium, July 10-17, 2019* (2019) [arXiv:1909.05652 \[hep-ph\]](#) .
- [21] J. Debove, B. Fuks, and M. Klasen, *Phys. Lett.* **B688**, 208 (2010), [arXiv:0907.1105 \[hep-ph\]](#) .
- [22] J. Debove, B. Fuks, and M. Klasen, *Nucl. Phys.* **B842**, 51 (2011), [arXiv:1005.2909 \[hep-ph\]](#) .
- [23] J. Debove, B. Fuks, and M. Klasen, *Nucl. Phys.* **B849**, 64 (2011), [arXiv:1102.4422 \[hep-ph\]](#) .
- [24] B. Fuks, M. Klasen, D. R. Lamprea, and M. Rothering, *JHEP* **10**, 081 (2012), [arXiv:1207.2159 \[hep-ph\]](#) .
- [25] B. Fuks, M. Klasen, D. R. Lamprea, and M. Rothering, *Proceedings, 37th International Conference on High Energy Physics (ICHEP 2014): Valencia, Spain, July 2-9, 2014*, *Nucl. Part. Phys. Proc.* **273-275**, 479 (2016), [arXiv:1407.7963 \[hep-ph\]](#) .
- [26] J. Fiaschi and M. Klasen, *Phys. Rev.* **D98**, 055014 (2018), [arXiv:1805.11322 \[hep-ph\]](#) .
- [27] B. Fuks, M. Klasen, and M. Rothering, *JHEP* **07**, 053 (2016), [arXiv:1604.01023 \[hep-ph\]](#) .
- [28] M. Klasen, B. Fuks, and M. Sunder, *Proceedings, 2017 European Physical Society Conference on High Energy Physics (EPS-HEP 2017): Venice, Italy, July 5-12, 2017*, *PoS EPS-HEP2017*, 298 (2017), [arXiv:1709.02680 \[hep-ph\]](#) .
- [29] B. Fuks, M. Klasen, F. Ledroit, Q. Li, and J. Morel, *Nucl. Phys.* **B797**, 322 (2008), [arXiv:0711.0749 \[hep-ph\]](#) .
- [30] T. Jezo, M. Klasen, D. R. Lamprea, F. Lyonnet, and I. Schienbein, *JHEP* **12**, 092 (2014), [arXiv:1410.4692 \[hep-ph\]](#) .
- [31] T. Jezo, M. Klasen, D. Lamprea, F. Lyonnet, and I. Schienbein, *Proceedings, 23rd International Workshop on Deep-Inelastic Scattering and Related Subjects (DIS 2015): Dallas, Texas, USA, April 27-May 01, 2015*, *PoS DIS2015*, 112 (2015).
- [32] M. Klasen, F. Lyonnet, and F. S. Queiroz, *Eur. Phys. J.* **C77**, 348 (2017), [arXiv:1607.06468 \[hep-ph\]](#) .
- [33] B. Fuks, M. Klasen, D. R. Lamprea, and M. Rothering, *Eur. Phys. J.* **C73**, 2480 (2013), [arXiv:1304.0790 \[hep-ph\]](#) .
- [34] G. Aad *et al.* (ATLAS), (2019), [arXiv:1909.09226 \[hep-ex\]](#) .
- [35] A. M. Sirunyan *et al.* (CMS), *Phys. Lett.* **B782**, 440 (2018), [arXiv:1801.01846 \[hep-ex\]](#) .
- [36] X. Cid Vidal *et al.* (Working Group 3), (2018), [arXiv:1812.07831 \[hep-ph\]](#) .
- [37] A. Vogt, *Phys. Lett.* **B497**, 228 (2001), [arXiv:hep-ph/0010146 \[hep-ph\]](#) .
- [38] N. Kidonakis, *Int. J. Mod. Phys.* **A19**, 1793 (2004), [arXiv:hep-ph/0303186 \[hep-ph\]](#) .
- [39] N. Kidonakis, *Phys. Rev.* **D77**, 053008 (2008), [arXiv:0711.0142 \[hep-ph\]](#) .

- [40] W. Beenakker, R. Hopker, M. Spira, and P. M. Zerwas, *Nucl. Phys.* **B492**, 51 (1997), [arXiv:hep-ph/9610490 \[hep-ph\]](#) .
- [41] W. Beenakker, M. Kramer, T. Plehn, M. Spira, and P. M. Zerwas, *Nucl. Phys.* **B515**, 3 (1998), [arXiv:hep-ph/9710451 \[hep-ph\]](#) .
- [42] W. Beenakker, C. Borschensky, M. Kramer, A. Kulesza, E. Laenen, V. Theeuwes, and S. Thewes, *JHEP* **12**, 023 (2014), [arXiv:1404.3134 \[hep-ph\]](#) .
- [43] W. Beenakker, C. Borschensky, R. Heger, M. Kramer, A. Kulesza, and E. Laenen, *JHEP* **05**, 153 (2016), [arXiv:1601.02954 \[hep-ph\]](#) .
- [44] W. Beenakker, C. Borschensky, M. Kramer, A. Kulesza, and E. Laenen, *JHEP* **12**, 133 (2016), [arXiv:1607.07741 \[hep-ph\]](#) .
- [45] G. F. Sterman, *Nucl. Phys.* **B281**, 310 (1987).
- [46] S. Catani and L. Trentadue, *Nucl. Phys.* **B327**, 323 (1989).
- [47] O. V. Tarasov, A. A. Vladimirov, and A. Yu. Zharkov, *Phys. Lett.* **93B**, 429 (1980).
- [48] S. A. Larin and J. A. M. Vermaseren, *Phys. Lett.* **B303**, 334 (1993), [arXiv:hep-ph/9302208 \[hep-ph\]](#) .
- [49] S. Moch, J. A. M. Vermaseren, and A. Vogt, *Nucl. Phys.* **B726**, 317 (2005), [arXiv:hep-ph/0506288 \[hep-ph\]](#) .
- [50] H. Contopanagos and G. F. Sterman, *Nucl. Phys.* **B419**, 77 (1994), [arXiv:hep-ph/9310313 \[hep-ph\]](#) .
- [51] S. Catani, M. L. Mangano, P. Nason, and L. Trentadue, *Nucl. Phys.* **B478**, 273 (1996), [arXiv:hep-ph/9604351 \[hep-ph\]](#) .
- [52] A. D. Martin, W. J. Stirling, R. S. Thorne, and G. Watt, *Eur. Phys. J.* **C63**, 189 (2009), [arXiv:0901.0002 \[hep-ph\]](#) .
- [53] S. Dulat, T.-J. Hou, J. Gao, M. Guzzi, J. Huston, P. Nadolsky, J. Pumplin, C. Schmidt, D. Stump, and C. P. Yuan, *Phys. Rev.* **D93**, 033006 (2016), [arXiv:1506.07443 \[hep-ph\]](#) .
- [54] C. F. Berger, J. S. Gainer, J. L. Hewett, and T. G. Rizzo, *JHEP* **02**, 023 (2009), [arXiv:0812.0980 \[hep-ph\]](#) .
- [55] B. Fuks, M. Klasen, S. Schmiemann, and M. Sunder, *Eur. Phys. J.* **C78**, 209 (2018), [arXiv:1710.09941 \[hep-ph\]](#) .